Heliyon 9 (2023) e17250

Contents lists available at ScienceDirect

Heliyon

journal homepage: www.cell.com/heliyon

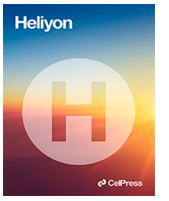

Biosorption of aqueous Pb(II) by H_3PO_4-activated biochar prepared from palm kernel shells (PKS)

Wipawee Dechapanya [a,b], Attaso Khamwichit [a,b,*]

[a] School of Engineering and Technology, Walailak University, 222 Thaiburi, Thasala, Nakhon Si Thammarat, 80160 Thailand
[b] Biomass and Oil Palm Center of Excellence, Walailak University, 222 Thaiburi, Thasala, Nakhon Si Thammarat, 80160 Thailand

ARTICLE INFO

Keywords:
Activated biochar
Palm kernel shells
Biosorbent
Biosorption
Heavy metals adsorption

ABSTRACT

The conversion of palm kernel shells (PKS), a major agricultural waste from the palm oil sector, into a potentially high-value biosorbent for heavy metals-contaminated wastewater treatments was explored in this work. Following carbonization, the activated PKS was chemically activated by soaking the biochar in a phosphoric acid (H_3PO_4) solution at 25 °C. The low-temperature approach benefits from less dangerous acid fume production and operational challenges when compared to the high-temperature procedure. The properties of the biochar were characterized by BET, FTIR, and SEM. The effects of H_3PO_4 dosage, initial Pb(II) concentration, and adsorbent dosage on removing Pb(II) from synthetic wastewater were investigated in the adsorption study. The activation of PKS biochar with high H3PO4 concentrations led to enhanced removal efficiency. The pseudo-second-order (PSO) kinetic model fitted the experimental data well (R^2 0.99), indicating that chemisorption was likely involved in the adsorption of Pb(II) onto activated PKS. Pb(II) sorption was possibly promoted by the presence of phosphate moieties on the adsorbent surface. The Langmuir isotherm best described the sorption of Pb(II) onto the activated PKS (R^2 0.97), giving the calculated maximum adsorption capacity (q_m) of 171.1 μg/g. In addition to physical sorption, possible adsorption mechanisms included functional group complexation and surface precipitation. Overall, activating PKS biochar with H_3PO_4 at room temperature could be a promising technique to improve the adsorbent's adsorption efficiency for Pb(II) removal from wastewater.

1. Introduction

Heavy metal contamination in water leads to both human health and environmental impacts, including effects on human metabolism [1], neuronal damage, cardiovascular disorders, renal injuries, and risk of cancer and diabetes [2]. Among harmful heavy metals, lead (Pb) is one of the high-potential threats to human health associated with the digestion of contaminated drinking water [3]. According to the U.S. EPA (2023), the maximum concentrations for the heavy metals contaminated in drinking water are Hg (0–002 mg/L), Pb (0–015 mg/L), Cr (0–1 mg/L), Cu (1–3 mg/L), Cd (0–005 mg/L) and Zn and Ni (0–04 mg/L). However, the lead concentration in water has exceeded the recommended limits in many regions of the world, especially in developing countries. Primary sources of heavy metals including Pb (lead) in drinking water are industrialization, urbanization, the growth of population, and

* Corresponding author. School of Engineering and Technology, Walailak University, 222 Thaiburi, Thasala, Nakhon Si Thammarat, 80160 Thailand.
E-mail address: kattaso@mail.wu.ac.th (A. Khamwichit).

https://doi.org/10.1016/j.heliyon.2023.e17250
Received 30 March 2023; Received in revised form 11 June 2023; Accepted 12 June 2023
Available online 7 July 2023

agricultural activities [4,5]. Wastewater discharges from these sources can elevate heavy metals in various water bodies leading to heavy metal exposure via drinking water. Several practical approaches for wastewater remedies to remove heavy metal traces have been reported [6,7]. Among these, novel procedures and materials that help in the finding and elimination of specific heavy metals have been developed and caught attention lately, especially bio-absorbent [8–10]. Bio-adsorption is more economical compared to other methods, has more flexibility in operation for a wide range of metal contaminants, and has less sludge volume. Nonetheless, the removal of metals using the adsorption method crucially depends on adsorbent performance [11–13]. Many recent research studies have focused on developing bio-adsorbent materials from various types of biomass [14].

Biochar has the potential to be a widely used material to clean up water and soil contamination due to its wide availability of feedstocks and favorable physical and chemical surface properties [15–17]. Characteristics of biochar, such as ion-exchange capability, surface groups, and pore size distribution all play a role in how well biochar removes pollutants. In general, biochar has several functional groups and high porosity [18]. To successfully remediate organic pollutants, biochar must be created at relatively high pyrolysis temperatures. This increases surface area, hydrophobicity, and microporosity. The removal of polar organic and inorganic contaminants via oxygen-containing functional groups, precipitation, and electrostatic attraction is thought to be more effective with biochar produced at lower temperatures [19,20]. Besides pollution remediation, biochar can potentially be used in soil fertility improvement through lime action due to its enrichment in the volatile matter and ability to increase pore volume, and carbon dioxide removal from the atmosphere [21]. Additionally, nanomaterials based on biochar have demonstrated strong photocatalytic capabilities in the destruction of organic contaminants [22,23].

Palm Kernel Shell (PKS) is very attractive as a valuable biomass from palm oil industries. This is because PKS is highly utilized in both energy and environmental aspects. PKS is one of the inexpensive biomasses and is abundantly available across Southeast Asia. Biochar from PKS can be obtained through the pyrolysis process. Product yields and composition from biomass pyrolysis depend on the operating conditions such as types of biomasses, time, temperature, and heating rate [24]. Pristine biochar, a byproduct of biomass pyrolysis, has been widely used as a bio-adsorbent; however, its specific surface area is relatively low [25]. Therefore, activation is implemented to improve the physical characteristics of the biochar which results in enhanced absorption capacity [26]. In practice, activation can be achieved by both physical and chemical methods. For physical activation, air or steam, or CO_2 is applied as the activation agent. During physical activation, the most volatile carbon of biochar can be removed, and the pore can be diffused with others resulting in the enhancement of the specific surface area and a sturdy microporous structure [27]. Whereas chemical activation uses a chemical activating agent in a high-temperature process, typically in a range of 450–900 °C [28]. Acid, alkali, and oxidation treatment are primarily used as activating agents. The advantages of chemicals compared to physical activation are as followed; higher surface area, lower operating temperature, higher efficiency, and better microporosity of biochar [29].

Among available acid-activated reagents, the advantages of phosphoric acid (H_3PO_4) over other reagents include less environmental effect and simplicity of recovery [30]. In addition, employing H_3PO_4 is highly recommended for the acid activation of biochar because it enables impregnation at room temperature and improves mesoporous characteristics [31,32]. The phosphorus species formed in activated biochar also have the potential to alter and regulate the textural properties and structures of biochar [33].

Once the adsorption equilibrium has been reached, the biochar adsorbent can be regenerated for possible reuse. The main regeneration concepts used in biochar regeneration are adsorbate desorption and adsorbate decomposition. By using various technologies to treat various types of biochar, regeneration of biochar and cost reduction can be accomplished. These technologies include thermal regeneration, solvent regeneration, microwave irradiation regeneration, and superficial fluid regeneration [34]. Every cycle of regeneration generally results in a decline in the effectiveness of adsorption, and the degree of reusability is heavily influenced by the type of biochar and the regeneration conditions [35].

Despite numerous studies on the improved adsorption capacity of various chemically-activated biochar, the improvement in heavy metal adsorption of PKS biochar activated with H_3PO_4 via a two-step process has received little attention elsewhere. It would be interesting to investigate the use of environmentally friendly phosphoric acid as the activating agent to improve the adsorption performance of PKS biochar. In this study, the H_3PO_4 solution was used for low-temperature chemical activation after the carbonization step. The low-temperature approach benefits from less dangerous acid fume production and operational challenges when compared to the high-temperature procedure. The adsorption efficiency of Pb(II) removal from synthetic wastewater onto activated PKS was then investigated to determine biochar's potential as an effective adsorbent for heavy metal-contaminated wastewater treatment. The adsorption kinetics and isotherm analysis were performed to provide insight into the involved adsorption mechanisms.

2. Materials and methods

2.1. Biochar preparation

PKS obtained from oil palm industries were cleaned to rid of palm fiber before being dehydrated under the sun for at least 24 h, followed by baking at 105 °C for 24 h in the oven. Dried PKS were pyrolyzed at 400–500 °C for 3 h and cooled down at room temperature before being pulverized and sieved for the sizes 250 and 850 mm. For the chemical activation of biochar, 85% V/V H_3PO_4 purchased from Sigma Aldrich was used to prepare 500 ml of 45, 65, and 85% V/V solution. Crushed biochar with the amount of 150 g at the specific size was soaked into 300 ml of the prepared phosphoric acid solution for 24 h. After that activated biochar was washed thoroughly with water 3 times before adjusting pH to 7 using distilled water. Finally, activated biochar was dried in the oven at 105 °C for 24 h.

2.2. Characterization of activated biochar

The physical and chemical properties of the prepared biochar were analyzed by several techniques. The morphological properties were examined by scanning electron microscopy (SEM) equipped with energy dispersive X-ray analysis (EDX) (Zeiss Merlin VP compact, Germany). Image scanning and electron mapping were carried out at 5 and 10 kV, respectively, with an X-ray radiation source. The SEM images were taken at 5Kx magnification. Pore properties and BET surface areas were analyzed by nitrogen adsorption-desorption isotherm at 77 K (ASAP2460, Micromeritics, USA). For BET analysis, the samples were degassed at 80 °C for 5 h. An ATR-FTIR spectroscopy (TENSOR 27, Bruker) was used to investigate the adsorbent's functional groups in a wavelength range of 500–4000 cm^{-1} with a resolution of 2.0 cm^{-1}. Each spectrum was collected from an average of 4 scans with a scanning rate of 0.2 cm^{-1}/s.

2.3. Preparation of synthetic wastewater

All chemicals used in this study were commercial grade, purchased from Sigma Aldrich. Commercial $Pb(NO_3)$, in HNO_3 standards of 1,000 mg Pb/L, was dissolved in distilled water to prepare the aqueous solutions with the desired concentration of 11.67, 19.15, 33.77, 42.51, and 51.1 mg/L, respectively. The solution was adjusted by adding 0.1 M NaOH until the pH value of 7 was achieved.

2.4. Batch adsorption studies

For the investigation of Pb(II) removal using the activated PSK biochar, four sets of batch experiments were set up. In the first set of experiments, 10 g of 0, 45, 65, and 85% H_3PO_4 activated biochar with the size of 250 mm was used in the study of Pb(II) removal from the initial Pb(II) concentration of 11.67 mg/L. The second set of experiments was to study the effect of Pb(II) initial concentration on removal efficiency. Pb(II) initial concentration in the range of 11.67–51.1 mg/L was applied using 10 g of 85% H_3PO_4 activated biochar with the size of 250 and 850 μm. The third set of experiments was conducted to study the effect of absorbent size on Pb(II) removal. 10 g of 85% H_3PO_4 activated biochar with the size of 250 and 850 μm was used with the initial Pb(II) concentration of 11.67 mg/L. The fourth set of experiments was performed to test the effect of the adsorbent amount used. Various amounts of 85% H_3PO_4-activated biochar in the range of 10–50 g were utilized while the initial concentration of Pb(II) was 11.67 mg/L and the adsorbent size was 250 mm. A contact time of 180 min was applied in all sets of the experiment. The amount of 500 ml Pb(II) solution at various initial concentrations was prepared in a beaker. The H_3PO_4-activated biochar was then added to the beakers. During the batch experiments, the solutions were continuously shaken at 100 rpm in a shaking incubator. Samples were collected every minute from the beginning up to the first 10 min, after that the samples were collected every 5 min up to the first hour, then samples were collected every 10 min till the end of experiments (180 min). At a given time, approximately 15 ml of the solution was sampled out and filtered in a paper filtration unit in the following step. The Pb(II) concentration of the clear solution was then analyzed by Inductively Coupled Plasma, Optical Emission Spectroscopy (ICP-OES), PerkinElmer Avio200, USA.

2.5. Batch Pb(II) adsorption analysis

The adsorption capacity in terms of the amount of Pb(II) adsorbed was calculated using the mass balance equation, as shown in Eqn. (1):

Table 1
BET surface properties.

Feedstock	Description	BET Surface Area (m^2/g)	Pore Diameter (mm)	Total Pore Volume (cm^3/g)	Reference
Palm kernel shells (PKS)	0% H_3PO_4 activated biochar (average size 250 mm)	326.50	17.35	0.142	This work
	45% H_3PO_4 activated biochar (average size 250 mm)	318.25	17.69	0.141	
	65% H_3PO_4 activated biochar (average size 250 mm)	297.21	18.33	0.136	
	85% H_3PO_4 activated biochar (average size 250 mm)	310.36	18.29	0.142	
Palm kernel shells (PKS)	0% H_3PO_4 activated biochar (average size 850 mm)	210.35	18.04	0.091	This work
	45% H_3PO_4 activated biochar (average size 850 mm)	285.23	16.36	0.117	
	65% H_3PO_4 activated biochar (average size 850 mm)	181.72	17.54	0.080	
	85% H_3PO_4 activated biochar (average size 850 mm)	180.38	18.14	0.082	
Coconut shell	Char/H_3PO_4 = 0.3	n/a	n/a	0.652	[26]
Olive stones	Char/H_3PO_4 = 1.2	1,500	n/a	0.630	[37]
Organic sewage sludge	H_3PO_4 activated	289	2.65	0.436	[38]

$$q_e = (C_0 - C_e) / m \quad (1)$$

where q_e (mg/g) is the equilibrium concentration of Pb(II) adsorbed onto the biochar, C_o (mg/L) is the initial Pb(II) concentration in the solution, C_e (mg/L) is the equilibrium concentration in the solution, V (L) is a volume of the aqueous solution being tested, and m (g) is an adsorbent amount being used. The efficiency of Pb(II) removal was determined using Eqn. (2):

$$removal = (C_0 - C) / C_0 \quad (2)$$

The concentration data were collected from a batch adsorption experiment in an aqueous solution (pH = 7) with initial Pb(II) concentrations ranging from 11.67 to 51.10 mg/L using activated PSK biochar as the adsorbent. To investigate the rate-controlling mechanisms involved in the Pb(II) sorption process, the pseudo-first-order (PFO), pseudo-second-order (PSO), Elovich, and intra-particle diffusion (IPD) models were used in the kinetic study. For the adsorption isotherm analysis, the equilibrium concentration data was also linearly fitted with the Langmuir, Freundlich, Elovich, Temkin, and Dubinin-Radushkevich (D-R) models.

3. Results and discussion

3.1. Characterization of the biochar

Table 1 shows the surface area (S_{BET}, m^2/g), total pore volume (V_p, ml/g), and most probable pore size diameter (d, m) values for the biochar adsorbents. The specific surface area and total pore volume values for adsorbents treated with various acid concentrations (0, 45, 65, and 85% v/v) decreased slightly after phosphoric acid (H_3PO_4) treatment compared to those of untreated biochar. However, the pore size diameters of the modified samples tended to increase, particularly with increasing acid concentrations. This could be due to phosphoric acid decomposing the lignocellulose materials in biochar, causing morphological changes that increase the porosity of the biochar [36].

The FTIR spectra of the biochar samples are illustrated in Fig. 1. All of the biochar absorbents show similar spectra patterns with common band regions, including –OH stretching in hydroxy groups at 3377 cm^{-1}, aliphatic C–H stretching at 2920 cm^{-1}, C═O stretching vibration in carbonyl group at 1693 cm^{-1}, carboxylic C–O stretching at 1577 cm^{-1}, $–CH_3$ vibrations at 1380, and carboxylic C–O stretching at 879 cm^{-1} [39–41]. The peak appearing at 2350 cm^{-1} is possibly due to the presence of carbon dioxide trapped in the biochar samples [41]. The peak band at 1159 cm^{-1} is associated with C–O stretching vibration in a C–O–P linkage, suggesting that the acid modification could result in the formation of cellulose phosphate esters linked to the cellulose main chains [32,42,43]. The intensity of this peak is higher in samples activated with a higher concentration of H_3PO_4 solution, indicating that the biochar backbone and the presented phosphates have been esterified to a greater extent.

The morphology of the biochar was examined by SEM spectroscopy. As illustrated in Fig. 2, all biochar have similar porous structures with surface pores of varying sizes distributed across the surface. The fracture surface of the pristine biochar was clean, with sharp edge pores (Fig. 2a). However, the edge became rougher and etched in the acid-modified samples (Fig. 2b–d). During the activation process, phosphoric acid preferentially diffused into the outer shells of the adsorbent particles, where it reacted with the functional groups of the biochar and volatile matters [44]. Furthermore, the H_3PO_4 could dissolve soluble volatile matter and

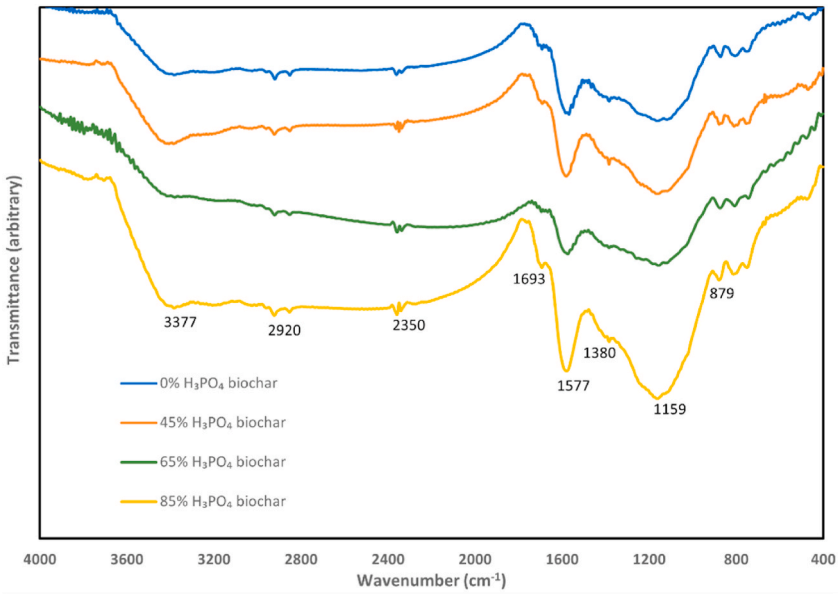

Fig. 1. FTIR spectra of the activated PKS biochar, treated with 0%, 45%, 65%, and 85% H_3PO_4.

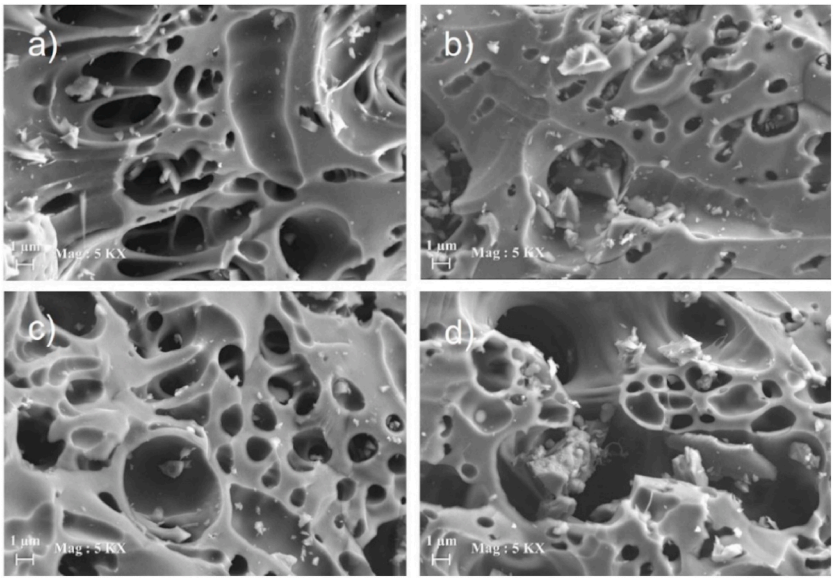

Fig. 2. SEM micrograph of a) 0% H_3PO_4 activated biochar, b) 45% H_3PO_4 activated biochar, c) 65% H_3PO_4 activated biochar, d) 85% H_3PO_4 activated biochar.

dissociate weakly bonded components (e.g., unstable carbons and volatile compounds) presented on the surface of the biochar. The elemental composition of the samples was also determined using EDX analysis, as shown in Fig. 3a–d. The phosphorus (P) and oxygen (O) contents of the activated biochar increased trendily with increasing concentrations of the phosphoric acid used in the solution after being activated by H_3PO_4. This could be an indication of the presence of phosphate entities incorporated onto the surface.

The results of the characterization of the H_3PO_4-activated PSK biochar show that the adsorbent has microporous structures with phosphate functional groups grafted to its surface and is capable of adsorbing the Pb(II) cations, which will be discussed in the

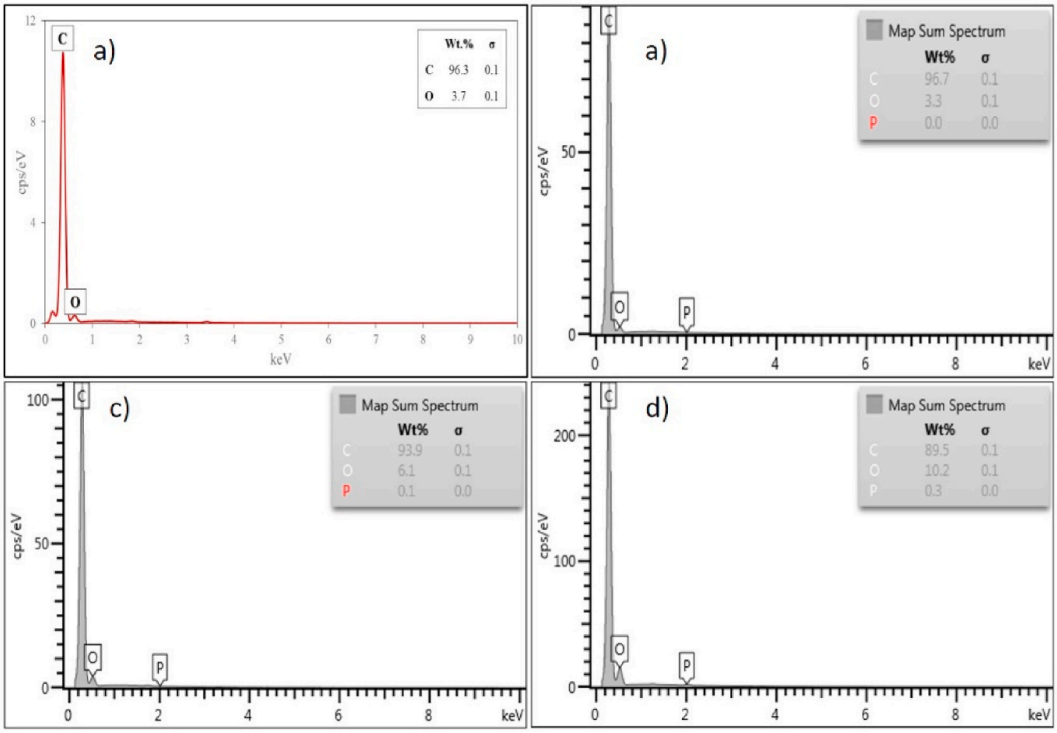

Fig. 3. EDX elemental analysis: a) 0% H_3PO_4 activated biochar, b) 45% H_3PO_4 activated biochar, c) 65% H_3PO_4 activated biochar, d) 85% H_3PO_4 activated biochar.

adsorption efficiency study.

3.2. Pb(II) equilibrium speciation

The effect of pH on lead speciation was predicted from the results obtained from MEDUSA® software [45]. The prediction of the specification of Pb in aqueous solutions is illustrated in Fig. 4. The speciation depicted by the software is presumably based on the equilibria species in an isolated homogeneous environment. From the diagram, Pb^{2+} and $Pb(OH)^{+}$ species are predominant at the studied pH of 7. These free Pb(II) cations preferentially compete for active sites that are available on the biochar surfaces on the sorption-desorption. The kinetic and isotherm of the adsorption for these free lead cations onto the adsorbent will be discussed later.

3.3. Adsorption efficiency of Pb(II) removal

As discussed earlier, treatment of the biochar by H_3PO_4 led to physical and chemical activation of the adsorbent surface to some extent. Fig. 5 shows the effect of the extent of H_3PO_4 activation of the biochar on the removal efficiency of Pb(II) from an aqueous solution. From the results, the adsorption efficiency of the adsorbent typically increased with the extent of chemical modification by the phosphoric acid. The adsorbents prepared by using a higher phosphoric acid concentration in the activation process resulted in higher removal efficiency. The Pb(II) sorption was promoted by H_3PO_4, possibly due to phosphate precipitation occurring during the ongoing adsorption [46,47], coupled with the formation of the associated Pb(II)-PO_4^{3-} complexes on the biochar surface [48]. According to the FTIR and EDX results, the H_3PO_4-activated PSK biochar had phosphate moieties grafted onto the particle surface, which was able to interact with the Pb(II) cations, resulting in precipitation. In comparison to pristine biochar, the adsorption capacity is determined solely by the physical sorption of Pb(II) onto the porous surface of the adsorbent particles and other chemisorption induced by associated interactions with the intrinsic functional groups, primarily the carboxylic and hydroxyl groups. The adsorption results were in good agreement with the other studies [49–51].

Fig. 6a illustrates the effect of the initial concentration of the Pb(II) aqueous solution on the adsorption efficiency of the activated biochar with an average size of 250 mm (85% H_3PO_4 biochar). The adsorption rate was relatively high at the initial stage and then it gradually decreased until the equilibrium had been reached, where the removal efficiency tended to reach a plateau at a longer time. At a fixed dosage of the adsorbent, the removal efficiency decreased with the increasing initial Pb(II) concentrations. The restricted adsorption sites could become saturated after being fully occupied by the adsorbed Pb(II) [49]. The adsorbent was exhausted and could no longer adsorb excess lead cations available in the solution [52].

Fig. 6b depicts the effect of the initial concentration of the Pb(II) aqueous solution on the adsorption efficiency of the activated biochar with an average size of 850 mm (85% H_3PO_4 biochar). The efficiency of Pb(II) adsorption onto the 85% H_3PO_4 biochar adsorbent was relatively lower than those of the systems with 85% H_3PO_4 biochar (250 mm) at the same initial solution concentration. The adsorption appeared to undergo at a much slower rate when 85% H_3PO_4 biochar adsorbent with a larger particle size (850 mm) was used. As discussed earlier, the BET surface area value of the 85% H_3PO_4 biochar was lower than that of the 85% H_3PO_4 biochar. The adsorption sites could become limited on the outer surface of the particle. With large particles, the cations would have to diffuse through the porous structure inside the particle to reach the active sites where the adsorption took place.

As shown in Fig. 7, the Pb(II) removal efficiency was higher with an increase in adsorbent dosage in the early stage of the adsorption process. However, the Pb (II) removal efficiency was relatively close to 100% at a much longer time at which the equilibrium had reached. At higher dosages, the quantity of available active sites on the surface ready for adsorption increased, resulting in improved Pb(II) adsorption efficiency. At a longer time; however, the excess Pb(II) ions could be continuously diffusing into the adsorbent porous particles and were finally adsorbed onto those intraparticle active sites.

3.4. Adsorption kinetics

The kinetics of Pb(II) adsorption onto the biochar was investigated by linear regression analysis of the PFO, PSO, Elovich, and IPD kinetic models. The equations in the linearized form of these models are shown in Eqs. (3)–(6), respectively. The kinetic parameters were obtained from the slopes and intercepts, generated from the plot of the model equations.

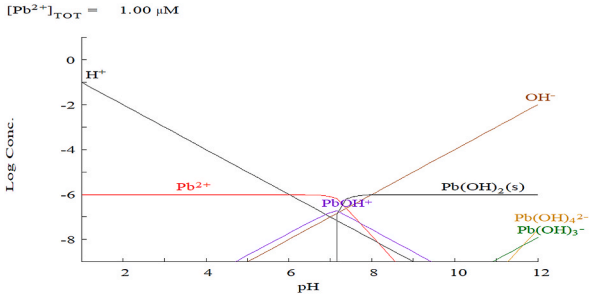

Fig. 4. Prediction of lead speciation in an aqueous solution generated by MEDUSA® software.

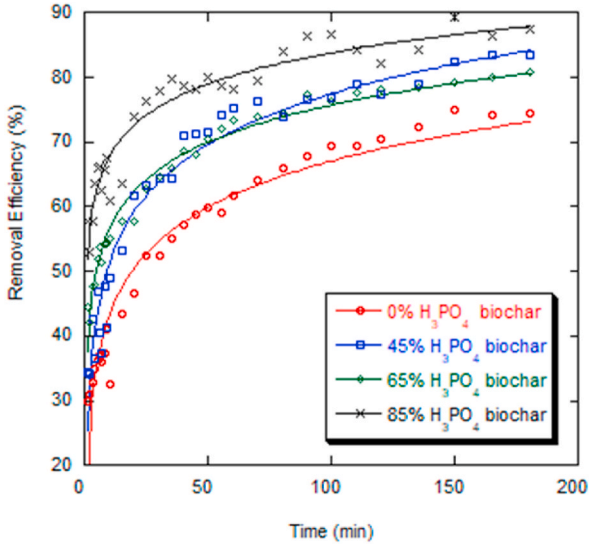

Fig. 5. Pb(II) removal efficiency of the activated biochar activated, treated with 0%, 45%, 65%, and 85% H_3PO_4.

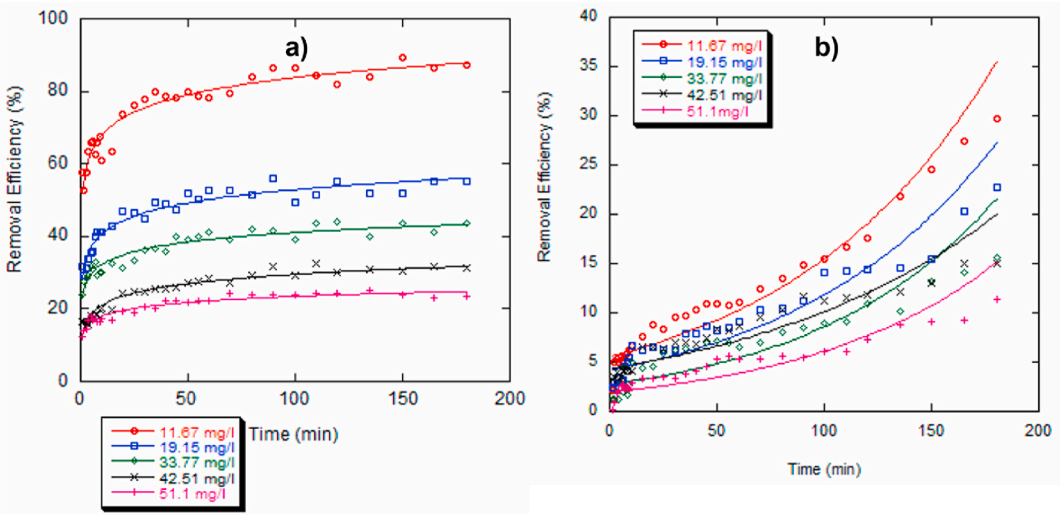

Fig. 6. The effect of the initial Pb(II) concentration of the solution on the removal efficiency of the activated biochar a) with an average size of 250 mm (85% H_3PO_4biochar), b) with an average size of 850 mm (85% H_3PO_4 biochar).

$$\text{PFO model}: \ln(q_e - q) = \ln(q_e) - k_1 t \tag{3}$$

$$\text{PSO model}: \frac{t}{q} = \frac{1}{k_2 q_e^2} + \frac{1}{q_e} t \tag{4}$$

$$\text{Elovich model}: q = \frac{1}{\beta}\ln(\alpha\beta) + \frac{1}{\beta}\ln(t) \tag{5}$$

$$\text{IPD model}: q = k_{\text{int}} t^{0.5} \tag{6}$$

Fig. 8a–d illustrates the regression analysis for the adsorption of Pb(II) onto the untreated (0% H_3PO_4) biochar and the acid-treated (45%, 65%, and 85% H_3PO_4) biochar. Table 2 summarizes the fitting parameters of the kinetic models described above. The PFO model assumes that the rate of adsorption is governed by physisorption in which the adsorption capacity is directly proportional to the concentration difference between the value at a given contact time and the equilibrium. Thus, the adsorption rate directly depends on the number of unoccupied adsorption sites. From the results, the PFO model was not well fitted to the experimental data for all adsorbents with the R^2 values of 0.73 for 0% H_3PO_4 biochar, 0.93 for 45% H_3PO_4 biochar, 0.83 for 65% H_3PO_4 biochar and 0.79 for 85%

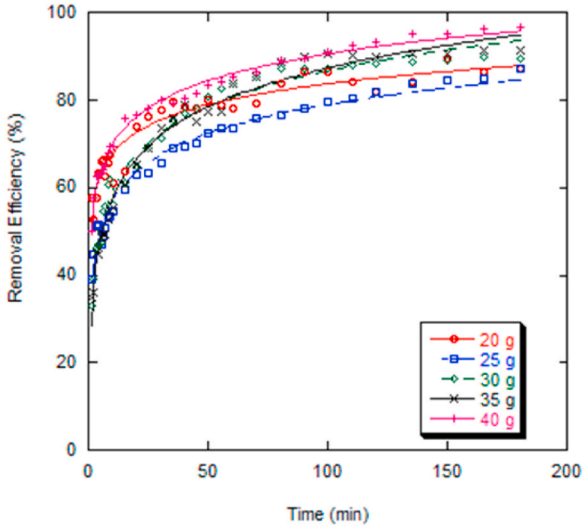

Fig. 7. The effect of adsorbent (85% H_3PO_4 biochar) dosage on the Pb(II) removal efficiency.

H_3PO_4 biochar, respectively. However, the experimental data fitted well with the PSO model, resulting in R^2 values of more than 0.99 for all adsorbents. The q_e values calculated from the regression analysis were very close to those obtained from the experiment. It suggested that the PSO model could appropriately describe the adsorption kinetics in which the chemisorption of the lead cations onto the biochar might be the rate-controlling mechanism. In addition, further investigation on the assumption of chemisorption onto the heterogeneous surface was tested by the Elovich model. Based on the model, α, ($mg.g^{-1}min^{-1}$) is the initial sorption rate, and the β ($g.mg^{-1}$) is the parameter related to the surface coverage and activation energy of chemisorption. From the results, the Elovich model was reasonably fitted to the experimental result with the R^2 values of 0.92 (0% H_3PO_4 biochar), 0.95 (45% H_3PO_4 biochar), 0.95 (65% H_3PO_4 biochar), and 0.97 (85% H_3PO_4 biochar), respectively. The initial adsorption rate was relatively high ($\alpha = 36.53$ mg/g.min) for the 85% H_3PO_4 biochar compared to those of the other adsorbents treated with lower acid concentrations. The results obtained from the PSO and Elovich models are in good agreement, suggesting that the chemisorption might be strongly involved in Pb(II) adsorption onto the biochar surfaces. From the regression analysis, the IPD model was invalid to describe the adsorption process, giving low R^2 values (0.60–0.90) for all adsorbents.

Fig. 9a–d depicts the regression analysis for the adsorption of Pb(II) onto 85% H_3PO_4 biochar with the size of 250 μm, for various initial Pb(II) concentrations. The fitting results are summarized in Table 3. The PSO kinetic model gave the best fittings to the experimental data (with R^2 values greater than 0.99) for all initial concentrations. The calculated q_e values for adsorption at different initial Pb concentrations were very close to the values obtained from the experiment. The adsorption rate (k_2) was likely to decrease with the increasing initial concentration. The Elovich model also resulted in reasonably good fittings with R^2 values in the range of 0.91 to 0.94. The results strongly suggested that Pb(II) adsorption onto biochar was chemisorption; however, the adsorption rate was affected by the solution's cation concentration.

3.5. Adsorption isotherms

The adsorption isotherms were analyzed to investigate the affinities of the adsorbed Pb(II) towards the activated biochar at the equilibrium that could provide insight into involved sorption mechanisms. The equilibrium data (298 K) measured from the adsorption of Pb(II) onto 85% H_3PO_4 biochar (250 μm) with a dosage of 20 g/500 ml solution were fitted into the following linear adsorption isotherm equations, including Langmuir (Eqn. (7)), Freundlich (Eqn. (8)), Elovich (Eqn. (9)), Temkin (Eqn. (10)), and Dubinin-Radushkevich (Eqn. (11)):

$$\text{Langmuir isotherm}: \frac{C_e}{q_e} = \frac{1}{q_m K_L} + \frac{C_e}{q_m} \tag{7}$$

$$\text{Freundlich isotherm}: \log(q_e) = \log(K_F) + (1/n)\log(C_e) \tag{8}$$

$$\text{Elovich isotherm}: \ln\left(\frac{q_e}{C_e}\right) = \ln(K_e q_m) - \frac{q_e}{q_m} \tag{9}$$

$$\text{Temkin isotherm}: q_e = B\ln(A_T) + B\ln(C_e) \tag{10}$$

$$\text{Dubinin} - \text{Radushkevich (D} - \text{R) isotherm}: \ln(q_e) = \ln(q_m) - \beta\varepsilon^2 \tag{11}$$

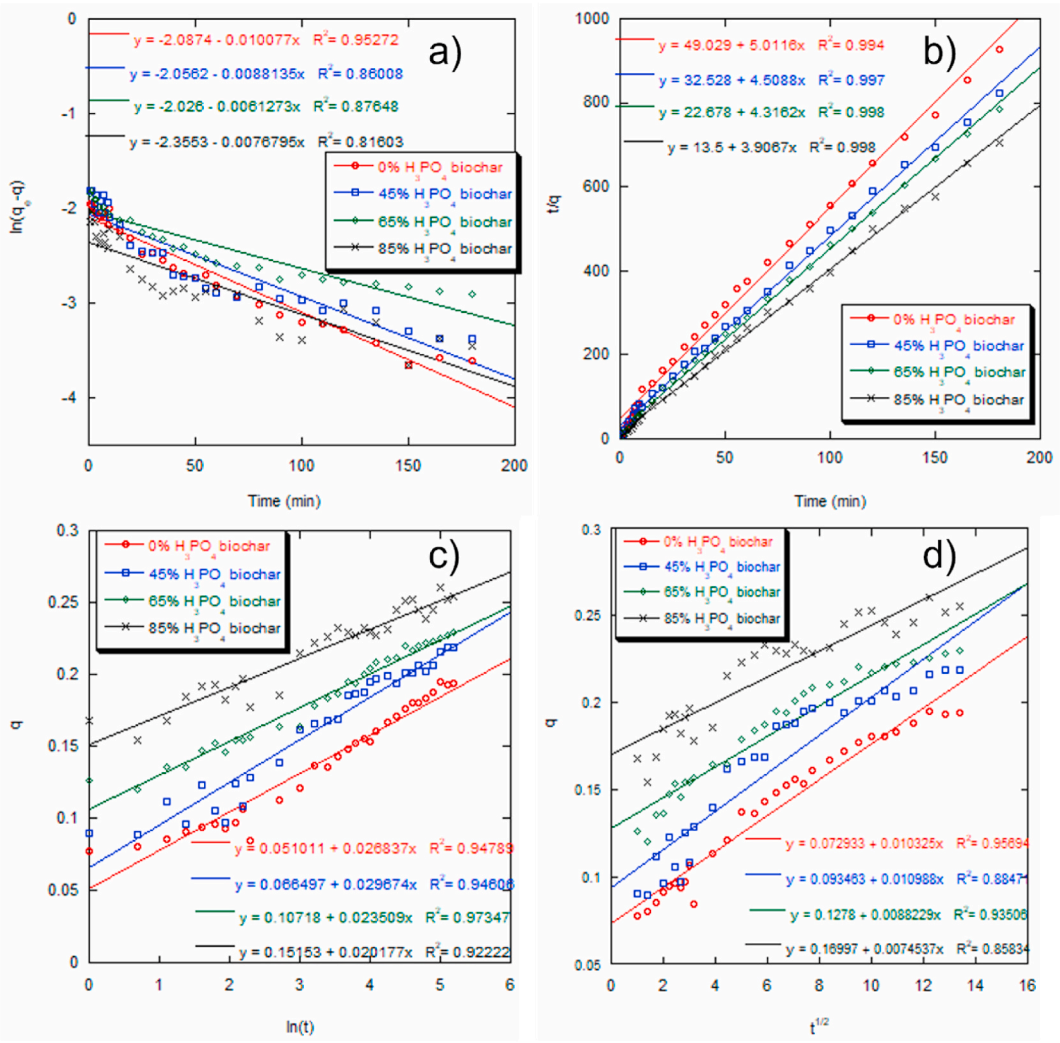

Fig. 8. The linear regression analysis of kinetic models a) SFO, b) SSO, Elovich, d) IPD for the adsorption of Pb(II) onto the untreated and H_3PO_4-treated biochars at 25 °C.

The parameters of the selected isotherms were determined from linear regression analysis. Fig. 10a–e shows the results from linear regression analysis of the studied models. Table 4 summarizes the adsorption parameters and the linear regression correlation coefficient (R^2) for the adsorption isotherms described above.

The Langmuir isotherm assumes the monolayer adsorption of the adsorbates onto the homogeneous surface with identical active sites takes place with no interaction between the species [53]. With an R^2 value of 0.9668, the Langmuir isotherm fitted well to the experimental data, giving an equilibrium constant (K_L) of 0.1149 L/mg and maximum adsorption capacity (q_m) of 0.1717 mg/g. The dimensionless separation factor (R_L) and surface coverage coefficient (θ) were calculated from Eqs. (12) and (13), respectively. The R_L value indicates the nature of adsorption equilibrium as follows: favorable isotherm ($0 < R_L < 1$), irreversible isotherm ($R_L = 0$), linear isotherm ($R_L = 1$), and unfavorable isotherm ($R_L > 1$) [54]. As illustrated in Fig. 11a, the separation factor (R_L) values were less than unity for the whole range of initial Pb(II) ion concentrations. From the graph, the R_L values decrease toward zero at higher initial concentrations, suggesting that the isotherm becomes more favorable and irreversible. The surface coverage coefficient can be proportionally related to the number of occupied adsorption sites at the equilibrium where the monolayer adsorption preferentially occurs. From Fig. 11b, the Pb(II) ions were able to get adsorbed onto the adsorbent at a greater surface coverage at higher initial concentrations. The higher the initial Pb(II) concentration was presented, the better dispersion for the monolayer adsorption on the adsorbent surface would be achieved. As the θ value reached about 0.85 (in the system with $C_0 = 51.51$ mg/L), most of the active sites were predominantly occupied by the adsorbed Pb(II) and fewer vacant sites were available for adsorption.

$$R_L = \frac{1}{1 + K_L C_0} \tag{12}$$

Table 2
Parameters for kinetic models of Pb(II) adsorption onto the biochar (250 μm).

Models	Adsorbent			
	0% H_3PO_4 biochar	45% H_3PO_4 biochar	65% H_3PO_4 biochar	85% H_3PO_4 biochar
Experimental q_e (mg/g)	0.1938	0.2190	0.2299	0.2549
PFO				
Calculated k_1 (min^{-1})	1.01×10^{-2}	8.81×10^{-3}	6.13×10^{-3}	7.68×10^{-3}
Calculated q_e (mg/g)	0.1240	0.1279	0.1319	0.0949
R^2	0.95	0.86	0.88	0.82
PSO				
k_2 (g/mg/min)	0.5123	0.6250	0.8215	1.1305
Calculated q_e (mg/g)	0.1995	0.2218	0.2317	0.2560
R^2	0.99	0.99	0.99	0.99
Elovich				
α (mg/g.min^{-1})	0.1795	0.2787	2.2451	36.7941
β (g/mg)	37.26	33.67	42.54	49.56
R^2	0.95	0.95	0.97	0.92
IPD				
k_{int} (mg/g/$min^{0.5}$)	1.03×10^{-2}	1.10×10^{-2}	8.82×10^{-3}	7.45×10^{-2}
C (mg/g)	7.29×10^{-2}	9.35×10^{-2}	1.28×10^{-1}	1.10×10^{-1}
R^2	0.96	0.88	0.94	0.86

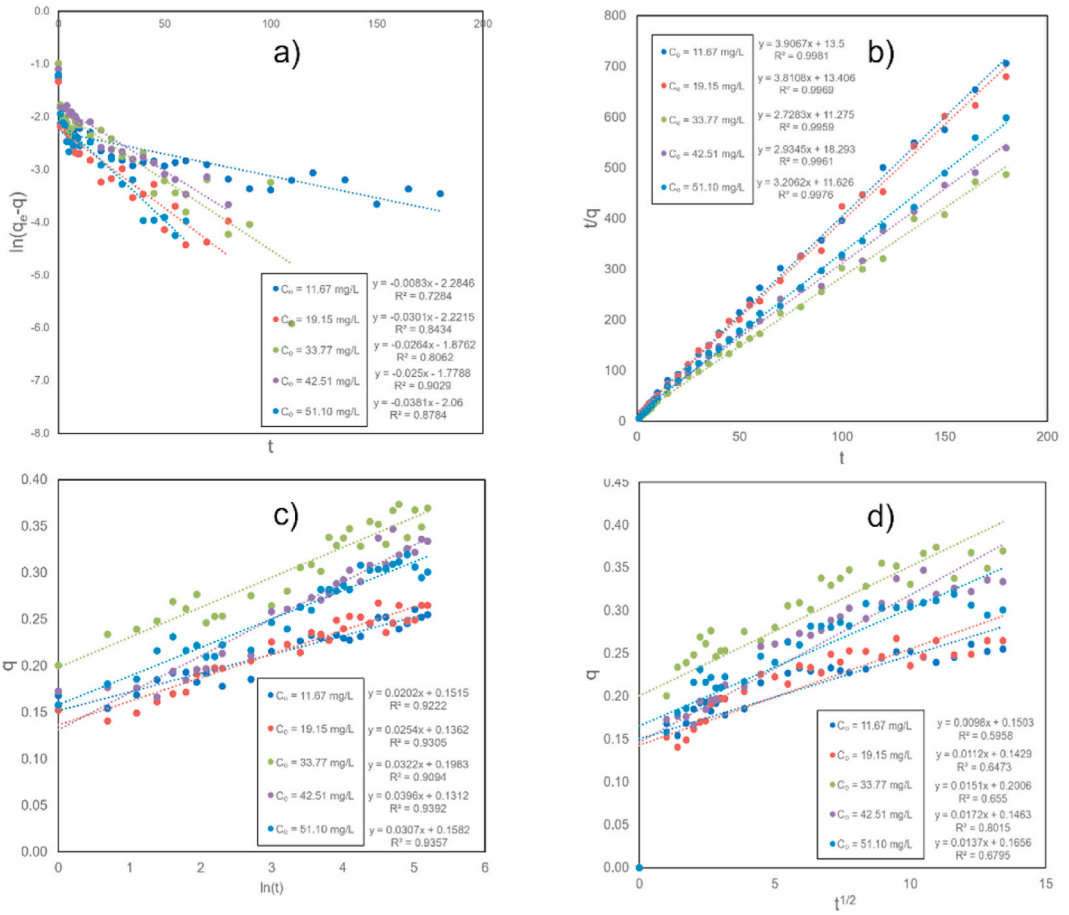

Fig. 9. The regression analysis of kinetic models: a) SFO, b) SSO, Elovich, d) IPD for the adsorption of Pb(II) onto the 85% H_3PO_4 biochar at 25 °C with different initial Pb(II) concentrations.

$$K_L C_0 = \frac{\theta}{1-\theta} \tag{13}$$

Table 3
Parameters for kinetic models of the Pb(II) adsorption from the solution with various initial concentrations.

Models	Initial Pb Concentration (mg/L)				
	11.67	19.15	33.77	42.51	51.10
Experimental q_e (mg/g)	0.2549	0.2648	0.3696	0.3339	0.3008
PFO					
Calculated k_1 (min^{-1})	8.3×10^{-3}	3.01×10^{-2}	2.64×10^{-2}	2.50×10^{-2}	3.81×10^{-3}
Calculated q_e (mg/g)	0.1018	0.1084	0.1532	0.1688	0.1275
R^2	0.73	0.84	0.83	0.90	0.89
PSO					
k_2 (g/mg/min)	1.1305	1.0833	0.6602	0.4707	0.5619
Calculated q_e (mg/g)	0.2560	0.2624	0.3665	0.3408	0.3119
R^2	0.99	0.99	0.99	0.99	0.99
Elovich					
α (mg/g.min^{-1})	36.52	5.42	15.22	1.09	5.31
β (g/mg)	49.51	39.37	31.06	25.25	32.57
R^2	0.92	0.93	0.91	0.94	0.94
IPD					
k_{int} (mg/g/$min^{0.5}$)	9.80×10^{-3}	1.12×10^{-2}	1.51×10^{-2}	1.72×10^{-2}	1.37×10^{-2}
C (mg/g)	1.50×10^{-1}	1.43×10^{-1}	2.01×10^{-1}	1.46×10^{-1}	1.66×10^{-1}
R^2	0.60	0.65	0.66	0.80	0.68

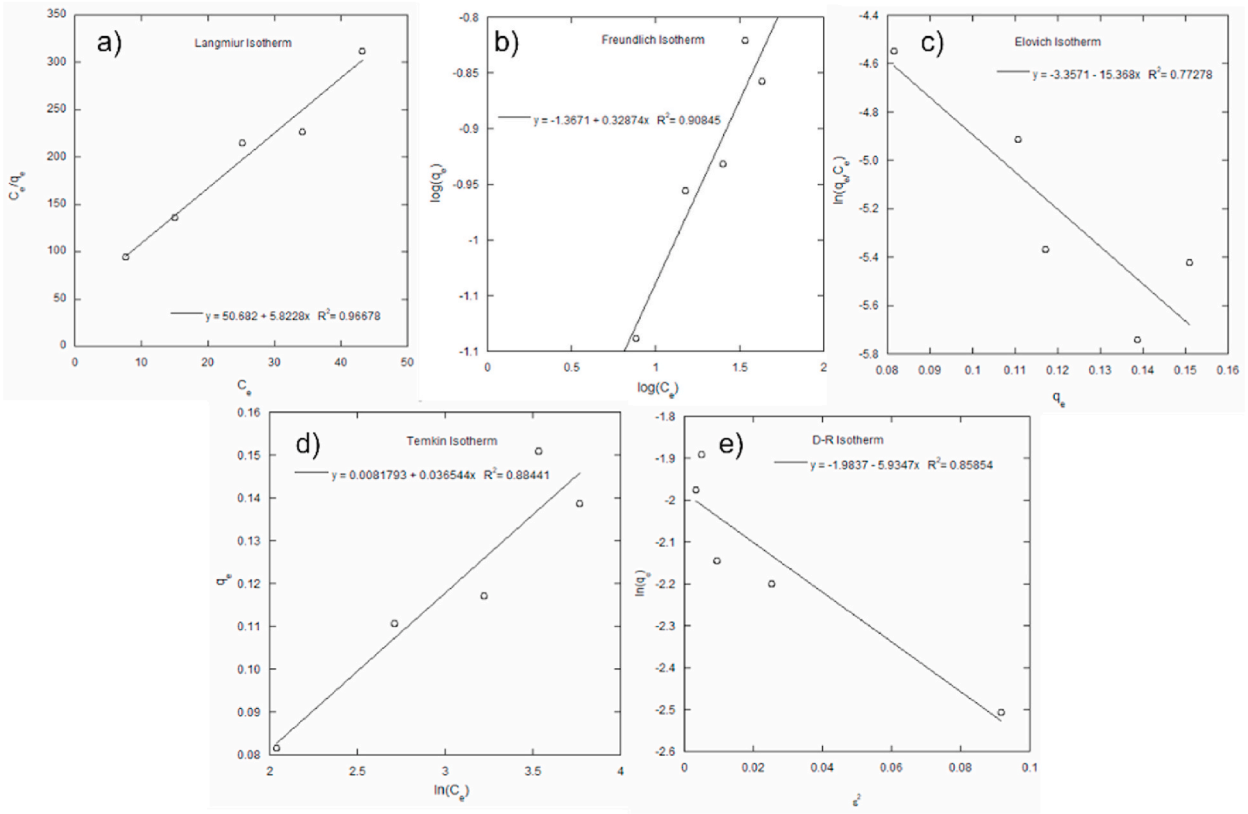

Fig. 10. The linear regression analysis of isotherm models for the adsorption of Pb(II) onto the 85% H_3PO_4 biochar at 25 °C with different initial Pb (II) concentrations: a) Langmuir, b) Freundlich, c) Elovich, d) Temkin, and d) Dubinin-Radushkevich (D–R) isotherm.

The Freundlich isotherm, based on multilayer adsorption on a heterogeneous surface [55], was applied to the adsorption fitting analysis. The model showed a reasonably good fit with the experimental data with a relatively high R^2 (0.9084), and a K_F value of 0.0429 (mg g^{-1})(L.mg^{-1})$^{1/n}$. The n value was calculated to be 3.04, suggesting favorable adsorption ($1 < n < 10$). As the n value is closer to zero, the heterogeneity of the adsorption is maximum [56]. From the results, it could be interpreted that the adsorption of the Pb(II) ions onto the heterogeneous surface of the 85% H_3PO_4-activated biochar adsorbent was favorable, and the separation of the sorbed species was relatively easy. In addition, the Elovich isotherm was examined to investigate the multilayer adsorption when the

Table 4
Isotherm model parameters.

Adsorption Isotherms	Model parameter
Langmuir	
slope = $1/q_m$	5.8228
q_m (mg.g^{-1})	0.1717
intercept = $1/q_mK_L$	50.6820
K_L (L.mg^{-1})	0.1149
R^2	0.97
Freundlich	
slope = 1/n	0.3287
n	3.0423
intercept = log (K_F)	−1.3671
K_F (mg.g^{-1})(L.mg^{-1})$^{1/n}$	0.0429
R^2	0.91
Elovich	
slope = $-1/q_m$	−15.368
q_m (mg.g^{-1})	0.0651
intercept = ln (K_eq_m)	−3.3571
K_e (L.mg^{-1})	0.5354
R^2	0.77
Temkin	
slope = B	0.0365
intercept = B*ln (A_T)	0.0082
b (kJ.mol^{-1})	67.8787
A_T (L.mg^{-1})	1.2519
R^2	0.88
Dubinin-Radushkevich (D-R)	
slope = -β	−5.9347
β	5.9347
intercept = ln (q_m)	−1.9837
q_m (mg.g^{-1})	0.1376
E (kJ.mol^{-1})	0.2903
R^2	0.86

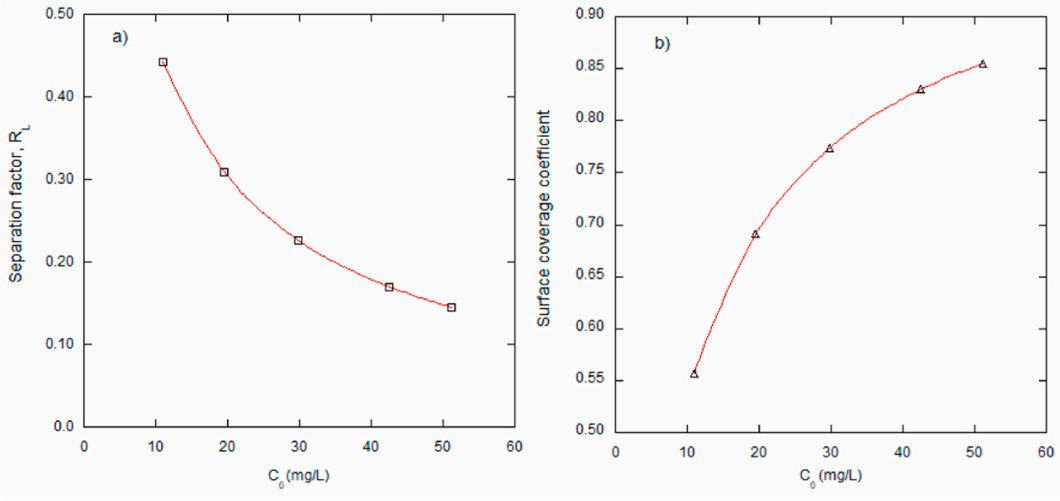

Fig. 11. Equilibrium Langmuir's parameter: a) separation factor (R_L), b) surface coverage (θ).

adsorption sites would increase exponentially with adsorption. However, the adsorption data did not fit well with the model with the R^2 value of 0.7728, giving the calculated q_m (0.0651 mg/g) and K_e (0.5354 L/mg), respectively.

The chemisorption mechanism could be involved to some extent in the adsorption process. The Temkin, D-R isotherm models were investigated to provide additional information regarding the interaction between the Pb(II) cations and the H_3PO_4-activated biochar. The model assumes the binding energy of the sorption largely depends on the surface coverage [57]. However, the results show that the Temkin model did not fit well with the experimental results with a low R^2 value (0.8844). The regression analysis gave the model parameter values A_T (1.2519 L/mg) and b (67.8787 kJ/mol). The high value of binding energy (b < 8 k J/mol) suggests that the chemisorption between the Pb(II) ions and the heterogeneous surface of the activated biochar could take part in the adsorption process

to some extent. The Dubinin-Radushkevich (D-R) isotherm assumes the adsorption takes place on the heterogeneous and porous surface [58]. The D-R model did not fit well with the adsorption data, having a relatively low R^2 value (0.8585), the adsorption energy coefficient (β) (5.9347 mol^2/J^2), the theoretical maximum capacity (q_m) (0.1376 mg/g), and the activation energy (E) (0.2903 kJ/mol).

3.6. Possible adsorption mechanisms

Pb(II) adsorption from aqueous solutions by biochar-based adsorbents could be controlled by physical and/or chemisorption mechanisms [59–62]. In this study, the sorption of Pb(II) onto the H_3PO_4-activated-PKS biochar could be attributed to several processes. Physical adsorption of Pb(II) onto the porous surface, complexation formation with functional groups, and possible phosphate precipitation all played important roles in the associated adsorption mechanisms, as shown in Fig. 12. From the characterization results, the activated biochar particles contain common carboxylic and hydroxyl functional groups as well as the phosphate linkage caused by the acid activation. As the sorption progressed, free Pb(II) diffused from the aqueous phase through the transport-resistant films and later became into contact with the reactive sites presented on the surface of the biochar particle. The Pb(II) could electrochemically interact with available carboxylic (-COOH) and hydroxyl (-OH) functional groups, resulting in functional group complexation [63]. Furthermore, the cations would be competitively precipitated with the PO_4^{3-} bonded on the heterogeneous surface of the phosphoric acid-activated PKS biochar [64]. Physical sorption may also occur concurrently, most likely on the outer wetted shell surrounding the porous adsorbent particles. However, the kinetic analysis strongly suggested that these chemisorptions were the rate-controlling step in the ongoing adsorption. When a low concentration of Pb(II) in the solution was present, the rate of adsorption appeared relatively fast, possibly due to less interference between neighboring molecules. The sorption proceeded until the process reached equilibrium, at which point the adsorbed Pb(II) monolayers formed on the heterogeneous surface of the particles.

4. Conclusions

The H_3PO_4-activated PKS biochar has shown great promise as a biosorbent for removing lead from contaminated wastewater. Chemical activation by phosphoric acid could potentially improve Pb(II) sorption by introducing phosphate precipitation during the adsorption process. Under the study conditions, the PKS biochar activated by 85% H_3PO_4 aqueous solution had the highest Pb(II) removal efficiency. The kinetic analysis revealed that the PSO model fit the experimental data well, implying that chemisorption was likely involved in the adsorption of Pb(II) onto the activated PKS adsorbent. The Langmuir isotherm best described the monolayer sorption of Pb(II) onto the heterogeneous active sites available at the adsorbent surface at equilibrium, with a maximum adsorption capacity qm of 171.7 μg/g.

PSK biochar can be produced on a large scale economically using today's technologies and environmentally friendly methods. PSK biochar can be produced on a large scale economically using today's technologies and environmentally friendly methods. The results of this study demonstrated that a simple two-step activation at low temperatures could improve the Pb(II) sorption capability of PKS biochar. This approach could become attractive and widely used for the production of environmentally friendly biosorbents from abundant biomass wastes.

Author's contribution

Wipawee Dechapanya, Ph.D.; Attaso Khamwichit, Ph.D.: Conceived and designed the experiments; Performed the experiments; Analyzed and interpreted the data; Contributed reagents, materials, analysis tools or data; Wrote the paper.

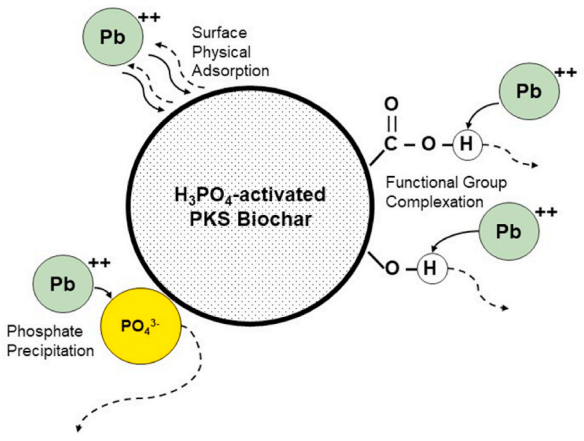

Fig. 12. Schematic illustration of possible Pb(II) adsorption mechanisms onto the H_3PO_4-activated PKS biochar.

Data availability

Data included in article/supp. material/referenced in the article.

Declaration of competing interest

The authors declare that they have no known competing financial interests or personal relationships that could have appeared to influence the work reported in this paper.

Acknowledgments

This work was financially funded by research grant number WUSTP-18/2665, Walailak University, Thailand. The authors would like to thank the Biomass and Oil Palm Center of Excellence (BoP-CoE), Walailak University, for facilitating support.

References

[1] Z. Fu, S. Xi, The effects of heavy metals on human metabolism, Toxicol. Mech. Methods 30 (2020) 167–176, https://doi.org/10.1080/15376516.2019.1701594.
[2] K. Rehman, F. Fatima, I. Waheed, M.S.H. Akash, Prevalence of exposure of heavy metals and their impact on health consequences, J. Cell. Biochem. 119 (2018) 157–184, https://doi.org/10.1002/jcb.26234.
[3] L. Järup, Hazards of heavy metal contamination, Br. Med. Bull. 68 (2003) 167–182, https://doi.org/10.1093/bmb/ldg032.
[4] R. Dixit, Wasiullah, D. Malaviya, K. Pandiyan, U. Singh, A. Sahu, R. Shukla, B. Singh, J. Rai, P. Sharma, H. Lade, D. Paul, Bioremediation of heavy metals from soil and aquatic environment: an overview of principles and criteria of fundamental processes, Sustainability 7 (2015) 2189–2212, https://doi.org/10.3390/su7022189.
[5] S.F. Ahmed, P.S. Kumar, M.R. Rozbu, A.T. Chowdhury, S. Nuzhat, N. Rafa, T.M.I. Mahlia, H.C. Ong, M. Mofijur, Heavy metal toxicity, sources, and remediation techniques for contaminated water and soil, Environ. Technol. Innov. 25 (2022), 102114, https://doi.org/10.1016/J.ETI.2021.102114.
[6] S. Babel, T.A. Kurniawan, Low-cost adsorbents for heavy metals uptake from contaminated water: a review, J. Hazard Mater. 97 (2003) 219–243, https://doi.org/10.1016/S0304-3894(02)00263-7.
[7] S.M. Lee, C. Laldawngliana, D. Tiwari, Iron oxide nano-particles-immobilized-sand material in the treatment of Cu(II), Cd(II) and Pb(II) contaminated waste waters, Chem. Eng. J. (2012) 103–111, https://doi.org/10.1016/J.CEJ.2012.04.075, 195–196.
[8] W.N. El-Sayed, K.Z. Elwakeel, A. Shahat, M.R. Awual, Investigation of novel nanomaterial for the removal of toxic substances from contaminated water, RSC Adv. 9 (2019) 14167–14175, https://doi.org/10.1039/C9RA00383E.
[9] M.N. Hasan, M.A. Shenashen, M.M. Hasan, H. Znad, M.R. Awual, Assessing of cesium removal from wastewater using functionalized wood cellulosic adsorbent, Chemosphere 270 (2021), https://doi.org/10.1016/J.CHEMOSPHERE.2020.128668.
[10] A. Khamwichit, W. Dechapanya, W. Dechapanya, Adsorption kinetics and isotherms of binary metal ion aqueous solution using untreated venus shell, Heliyon 8 (2022), e09610, https://doi.org/10.1016/J.HELIYON.2022.E09610.
[11] Y. Dai, N. Zhang, C. Xing, Q. Cui, Q. Sun, The adsorption, regeneration and engineering applications of biochar for removal organic pollutants: a review, Chemosphere 223 (2019) 12–27, https://doi.org/10.1016/j.chemosphere.2019.01.161.
[12] J.I.Z. Montero, A.S.C. Monteiro, E.S.J. Gontijo, C.C. Bueno, M.A. de Moraes, A.H. Rosa, High efficiency removal of As(III) from waters using a new and friendly adsorbent based on sugarcane bagasse and corncob husk Fe-coated biochars, Ecotoxicol. Environ. Saf. 162 (2018) 616–624, https://doi.org/10.1016/J.ECOENV.2018.07.042.
[13] R. Katiyar, A.K. Patel, T.B. Nguyen, R.R. Singhania, C.W. Chen, C. Di Dong, Adsorption of copper (II) in aqueous solution using biochars derived from Ascophyllum nodosum seaweed, Bioresour. Technol. 328 (2021), https://doi.org/10.1016/j.biortech.2021.124829.
[14] S.T. Akar, T. Akar, Z. Kaynak, B. Anilan, A. Cabuk, Ö. Tabak, T.A. Demir, T. Gedikbey, Removal of copper(II) ions from synthetic solution and real wastewater by the combined action of dried Trametes versicolor cells and montmorillonite, Hydrometallurgy 97 (2009) 98–104, https://doi.org/10.1016/J.HYDROMET.2009.01.009.
[15] M. Qiu, L. Liu, Q. Ling, Y. Cai, S. Yu, S. Wang, D. Fu, B. Hu, X. Wang, Biochar for the removal of contaminants from soil and water: a review, Biochar 4 (2022) 19, https://doi.org/10.1007/s42773-022-00146-1.
[16] L. Liang, F. Xi, W. Tan, X. Meng, B. Hu, X. Wang, Review of organic and inorganic pollutants removal by biochar and biochar-based composites, Biochar 3 (2021) 255–281, https://doi.org/10.1007/s42773-021-00101-6.
[17] M.D. Khan, T. Chottitisupawong, H.H.T. Vu, J.W. Ahn, G.M. Kim, Removal of phosphorus from an aqueous solution by nanocalcium hydroxide derived from waste bivalve seashells: mechanism and kinetics, ACS Omega 5 (2020) 12290–12301, https://doi.org/10.1021/acsomega.0c00993.
[18] P. Godlewska, H.P. Schmidt, Y.S. Ok, P. Oleszczuk, Biochar for composting improvement and contaminants reduction, A review, Bioresour Technol. 246 (2017) 193–202, https://doi.org/10.1016/j.biortech.2017.07.095.
[19] M. Qiu, L. Liu, Q. Ling, Y. Cai, S. Yu, S. Wang, D. Fu, B. Hu, X. Wang, Biochar for the removal of contaminants from soil and water: a review, Biochar 4 (2022) 19, https://doi.org/10.1007/s42773-022-00146-1.
[20] C.X. Yang, Q. Zhu, W.P. Dong, Y.Q. Fan, W.L. Wang, Preparation and characterization of phosphoric acid-modified biochar nanomaterials with highly efficient adsorption and photodegradation ability, Langmuir 37 (2021) 9253–9263, https://doi.org/10.1021/acs.langmuir.1c01468.
[21] A. Tomczyk, Z. Sokołowska, P. Boguta, Biochar physicochemical properties: pyrolysis temperature and feedstock kind effects, Rev. Environ. Sci. Biotechnol. 19 (2020) 191–215, https://doi.org/10.1007/s11157-020-09523-3.
[22] M. Qiu, B. Hu, Z. Chen, H. Yang, L. Zhuang, X. Wang, Challenges of organic pollutant photocatalysis by biochar-based catalysts, Biochar 3 (2021) 117–123, https://doi.org/10.1007/s42773-021-00098-y.
[23] M. Qiu, Z. Liu, S. Wang, B. Hu, The photocatalytic reduction of U(VI) into U(IV) by ZIF-8/g-C3N4 composites at visible light, Environ. Res. 196 (2021), 110349, https://doi.org/10.1016/j.envres.2020.110349.
[24] A.K. Sakhiya, A. Anand, P. Kaushal, Production, activation, and applications of biochar in recent times, Biochar 2 (2020) 253–285, https://doi.org/10.1007/s42773-020-00047-1.
[25] W.-J. Liu, H. Jiang, H.-Q. Yu, Development of biochar-based functional materials: toward a sustainable platform carbon, Material, Chem Rev. 115 (2015) 12251–12285, https://doi.org/10.1021/acs.chemrev.5b00195.
[26] M.J. Prauchner, F. Rodríguez-Reinoso, Chemical versus physical activation of coconut shell: a comparative study, Microporous Mesoporous Mater. 152 (2012) 163–171, https://doi.org/10.1016/j.micromeso.2011.11.040.
[27] N. Liu, A.B. Charrua, C.-H. Weng, X. Yuan, F. Ding, Characterization of biochars derived from agriculture wastes and their adsorptive removal of atrazine from aqueous solution: a comparative study, Bioresour. Technol. 198 (2015) 55–62, https://doi.org/10.1016/j.biortech.2015.08.129.
[28] P.M. Godwin, Y. Pan, H. Xiao, M.T. Afzal, Progress in preparation and application of modified biochar for improving heavy metal ion removal from wastewater, J. Bioresour. Bioprod. 4 (2019) 31–42, https://doi.org/10.21967/jbb.v4i1.180.
[29] A.K. Sakhiya, A. Anand, P. Kaushal, Production, activation, and applications of biochar in recent times, Biochar 2 (2020) 253–285, https://doi.org/10.1007/s42773-020-00047-1.

[30] Y. Luo, R. Li, X. Sun, X. Liu, D. Li, The roles of phosphorus species formed in activated biochar from rice husk in the treatment of landfill leachate, Bioresour. Technol. 288 (2019), 121533, https://doi.org/10.1016/J.BIORTECH.2019.121533.
[31] H. Niu, H. Jin, Q. Sun, Y. Shi, X. Zhang, Y. Cai, Activation of biochars by waste phosphoric acids: an integrated disposal route of waste acids and solid waste, ACS Sustain. Chem. Eng. 9 (2021) 16403–16414, https://doi.org/10.1021/acssuschemeng.1c06326.
[32] L. Cao, I.K.M. Yu, D.C.W. Tsang, S. Zhang, Y.S. Ok, E.E. Kwon, H. Song, C.S. Poon, Phosphoric acid-activated wood biochar for catalytic conversion of starch-rich food waste into glucose and 5-hydroxymethylfurfural, Bioresour. Technol. 267 (2018) 242–248, https://doi.org/10.1016/J.BIORTECH.2018.07.048.
[33] F. Yang, L. Sui, C. Tang, J. Li, K. Cheng, Q. Xue, Sustainable advances on phosphorus utilization in soil via addition of biochar and humic substances, Sci. Total Environ. 768 (2021), 145106, https://doi.org/10.1016/J.SCITOTENV.2021.145106.
[34] Y. Dai, N. Zhang, C. Xing, Q. Cui, Q. Sun, The adsorption, regeneration and engineering applications of biochar for removal organic pollutants: a review, Chemosphere 223 (2019) 12–27, https://doi.org/10.1016/J.CHEMOSPHERE.2019.01.161.
[35] T. Alsawy, E. Rashad, M. El-Qelish, R.H. Mohammed, A comprehensive review on the chemical regeneration of biochar adsorbent for sustainable wastewater treatment, NPJ Clean Water 5 (2022), https://doi.org/10.1038/s41545-022-00172-3.
[36] M.A. Naeem, A. Shabbir, M. Amjad, G. Abbas, M. Imran, B. Murtaza, M. Tahir, A. Ahmad, Acid treated biochar enhances cadmium tolerance by restricting its uptake and improving physio-chemical attributes in quinoa (Chenopodium quinoa Willd.), Ecotoxicol. Environ. Saf. 191 (2020), 110218, https://doi.org/10.1016/J.ECOENV.2020.110218.
[37] Y. Nakagawa, M. Molina-Sabio, F. Rodríguez-Reinoso, Modification of the porous structure along the preparation of activated carbon monoliths with H3PO4 and ZnCl2, Microporous Mesoporous Mater. 103 (2007) 29–34, https://doi.org/10.1016/j.micromeso.2007.01.029.
[38] J. Zhang, J. Shao, Q. Jin, Z. Li, X. Zhang, Y. Chen, S. Zhang, H. Chen, Sludge-based biochar activation to enhance Pb(II) adsorption, Fuel 252 (2019) 101–108, https://doi.org/10.1016/J.FUEL.2019.04.096.
[39] Y. Guo, R.M. Bustin, FTIR spectroscopy and reflectance of modern charcoals and fungal decayed woods: implications for studies of inertinite in coals, Int. J. Coal Geol. 37 (1998) 29–53, https://doi.org/10.1016/S0166-5162(98)00019-6.
[40] E. Fuente, J.A. Menéndez, M.A. Díez, D. Suárez, M.A. Montes-Morán, Infrared spectroscopy of carbon materials: a quantum chemical study of model compounds, J. Phys. Chem. B 107 (2003) 6350–6359, https://doi.org/10.1021/jp027482g.
[41] R. Md Salim, J. Asik, M.S. Sarjadi, Chemical functional groups of extractives, cellulose and lignin extracted from native Leucaena leucocephala bark, Wood Sci. Technol. 55 (2021) 295–313, https://doi.org/10.1007/s00226-020-01258-2.
[42] M.S. Solum, R.J. Pugmire, M. Jagtoyen, F. Derbyshire, Evolution of carbon structure in chemically activated wood, Carbon N Y 33 (1995) 1247–1254, https://doi.org/10.1016/0008-6223(95)00067-N.
[43] H. Hadoun, Z. Sadaoui, N. Souami, D. Sahel, I. Toumert, Characterization of mesoporous carbon prepared from date stems by H3PO4 chemical activation, Appl. Surf. Sci. 280 (2013) 1–7, https://doi.org/10.1016/J.APSUSC.2013.04.054.
[44] S.M. Taha, M.E. Amer, A.E. Elmarsafy, M.Y. Elkady, Adsorption of 15 different pesticides on untreated and phosphoric acid treated biochar and charcoal from water, J. Environ. Chem. Eng. 2 (2014) 2013–2025, https://doi.org/10.1016/J.JECE.2014.09.001.
[45] I. Puigdomenech, Hydra/Medusa chemical equilibrium database and plotting software. https://www.kth.se/che/medusa/downloads-1.386254, 2004. (Accessed 28 February 2022).
[46] L. Zhao, W. Zheng, O. Mašek, X. Chen, B. Gu, B.K. Sharma, X. Cao, Roles of phosphoric acid in biochar formation: synchronously improving carbon retention and sorption capacity, J. Environ. Qual. 46 (2017) 393–401, https://doi.org/10.2134/jeq2016.09.0344.
[47] Q. Ge, Q. Tian, S. Wang, J. Zhang, R. Hou, Highly efficient removal of lead/cadmium by phosphoric acid-modified hydrochar prepared from fresh banana peels: adsorption mechanisms and environmental application, Langmuir 38 (2022) 15394–15403, https://doi.org/10.1021/acs.langmuir.2c02693.
[48] Q. Shi, G.E. Sterbinsky, V. Prigiobbe, X. Meng, Mechanistic study of lead adsorption on activated carbon, Langmuir 34 (2018) 13565–13573, https://doi.org/10.1021/acs.langmuir.8b03096.
[49] D. Kołodyńska, R. Wnetrzak, J.J. Leahy, M.H.B. Hayes, W. Kwapiński, Z. Hubicki, Kinetic and adsorptive characterization of biochar in metal ions removal, Chem. Eng. J. 197 (2012) 295–305, https://doi.org/10.1016/J.CEJ.2012.05.025.
[50] W. Ahmed, S. Mehmood, A. Núñez-Delgado, S. Ali, M. Qaswar, A. Shakoor, M. Mahmood, D.-Y. Chen, Enhanced adsorption of aqueous Pb(II) by modified biochar produced through pyrolysis of watermelon seeds, Sci. Total Environ. 784 (2021), 147136, https://doi.org/10.1016/j.scitotenv.2021.147136.
[51] N. Zhou, H. Chen, J. Xi, D. Yao, Z. Zhou, Y. Tian, X. Lu, Biochars with excellent Pb(II) adsorption property produced from fresh and dehydrated banana peels via hydrothermal carbonization, Bioresour. Technol. 232 (2017) 204–210, https://doi.org/10.1016/j.biortech.2017.01.074.
[52] R. Kalaiarasi, E. Parameswari, V. Davamani, D.J.S. Sharmila, Exploring the potential of biochar activated with phosphoric acid towards hexavalent chromium removal, Int. Res. J. Pure Appl. Chem. (2020) 1–11, https://doi.org/10.9734/irjpac/2020/v21i2030278.
[53] R. Saadi, Z. Saadi, R. Fazaeli, N.E. Fard, Monolayer and multilayer adsorption isotherm models for sorption from aqueous media, Kor. J. Chem. Eng. 32 (2015) 787–799, https://doi.org/10.1007/s11814-015-0053-7.
[54] B.H. Hameed, A.A. Rahman, Removal of phenol from aqueous solutions by adsorption onto activated carbon prepared from biomass material, J. Hazard Mater. 160 (2008) 576–581, https://doi.org/10.1016/j.jhazmat.2008.03.028.
[55] G. Halsey, Physical adsorption on non-uniform surfaces, J. Chem. Phys. 16 (1948) 931–937, https://doi.org/10.1063/1.1746689.
[56] N. Mohammadi, H. Khani, V.K. Gupta, E. Amereh, S. Agarwal, Adsorption process of methyl orange dye onto mesoporous carbon material–kinetic and thermodynamic studies, J. Colloid Interface Sci. 362 (2011) 457–462, https://doi.org/10.1016/J.JCIS.2011.06.067.
[57] S. Chen, C. Qin, T. Wang, F. Chen, X. Li, H. Hou, M. Zhou, Study on the adsorption of dyestuffs with different properties by sludge-rice husk biochar: adsorption capacity, isotherm, kinetic, thermodynamics and mechanism, J. Mol. Liq. 285 (2019) 62–74, https://doi.org/10.1016/J.MOLLIQ.2019.04.035.
[58] M.A. Al-Ghouti, R.S. Al-Absi, Mechanistic understanding of the adsorption and thermodynamic aspects of cationic methylene blue dye onto cellulosic olive stones biomass from wastewater, Sci. Rep. 10 (2020), https://doi.org/10.1038/s41598-020-72996-3.
[59] H. Lu, W. Zhang, Y. Yang, X. Huang, S. Wang, R. Qiu, Relative distribution of Pb2+ sorption mechanisms by sludge-derived biochar, Water Res. 46 (2012) 854–862, https://doi.org/10.1016/J.WATRES.2011.11.058.
[60] Q. Ye, Q. Li, X. Li, Removal of heavy metals from wastewater using biochars: adsorption and mechanisms, Environ. Pollut. Bioavail. 34 (2022) 385–394, https://doi.org/10.1080/26395940.2022.2120542.
[61] H. Li, X. Dong, E.B. da Silva, L.M. de Oliveira, Y. Chen, L.Q. Ma, Mechanisms of metal sorption by biochars: biochar characteristics and modifications, Chemosphere 178 (2017) 466–478, https://doi.org/10.1016/J.CHEMOSPHERE.2017.03.072.
[62] G. Yin, X. Chen, B. Sarkar, N.S. Bolan, T. Wei, H. Zhou, H. Wang, Co-adsorption mechanisms of Cd(II) and As(III) by an Fe-Mn binary oxide biochar in aqueous solution, Chem. Eng. J. 466 (2023), 143199, https://doi.org/10.1016/J.CEJ.2023.143199.
[63] M. Qiu, L. Liu, Q. Ling, Y. Cai, S. Yu, S. Wang, D. Fu, B. Hu, X. Wang, Biochar for the removal of contaminants from soil and water: a review, Biochar 4 (2022) 19, https://doi.org/10.1007/s42773-022-00146-1.
[64] H. Peng, P. Gao, G. Chu, B. Pan, J. Peng, B. Xing, Enhanced adsorption of Cu(II) and Cd(II) by phosphoric acid-modified biochars, Environ. Pollut. 229 (2017) 846–853, https://doi.org/10.1016/j.envpol.2017.07.004.